ELSEVIER

Catalysis Today 53 (1999) 583–596

CATALYSIS TODAY

www.elsevier.com/locate/cattod

Mathematical modelling of catalytic monolithic reactors with storage of reaction components on the catalyst surface

Jiří Jirát [a,*], Milan Kubíček [b], Miloš Marek [a]

[a] *Department of Chemical Engineering, Center for Nonlinear Dynamics of Chemical and Biological Systems, Prague Institute of Chemical Technology, 166 28 Prague 6, Czech Republic*

[b] *Department of Mathematics, Center for Nonlinear Dynamics of Chemical and Biological Systems, Prague Institute of Chemical Technology, 166 28 Prague 6, Czech Republic*

Abstract

Effects of periodic switching between lean and rich combustion conditions on CO, HC and NO_x conversion on a monolithic catalyst with NO_x storage were simulated by mathematical model. The model includes description of oxygen and NO_x storage on the washcoat. Parametric study showed possibility to reach much improved time-averaged NO_x conversion on a single monolith in comparison with steady-state operation, but lower CO and HCs conversions under reducing (rich) conditions. Sequence of monoliths, the first one with NO_x storage catalyst and the second one with oxidizing catalyst, then enables to obtain satisfactory conversions of all pollutants.

Keywords: Periodic operation; Mathematical modelling; NO_x storage; Oxygen storage; Catalytic monolith reactor

1. Introduction

The number of mobile sources of exhaust gases is increasing and detoxification of emissions is still very important problem. The old problem — how to achieve oxidation of CO and HC simultaneously with NO_x reduction — was for gasoline engines practically solved by keeping the air/fuel ratio on stoichiometric level with classical three-way catalysts (TWC). This method cannot be used for more effective lean-burn engines (both diesel and gasoline), where relatively great excess of oxygen hinders catalytic reduction of NO_x. Besides, increasingly strict CO, HC and NO_x emission requirements there is also growing demand to minimize CO_2 emissions. Thus, the popularity of more efficient lean-burn engines is increasing. Hence intensive research on new catalysts for decomposition of NO_x under lean conditions — either direct or with the use of reductants (e.g. hydrocarbons) is now underway, cf. e.g. [1].

One of the new techniques for NO_x removal is based on 'NO_x storage' properties of novel catalysts [2]. These are Pt-based catalysts which contain earth-alkaline metals, mainly Ba. Under excess oxygen, NO reacts with oxygen and the resulting NO_x react with Ba to form nitrates (NO_x are stored on the surface). Under reducing conditions the nitrates are reduced by reductants (CO, H_2 or HCs) to nitrogen or nitrous oxide. Hence the periodic operation, including switching between lean-burn and rich-burn combustion phases, could enable proper storage and operating conditions to improve significantly time-averaged NO_x conversion [2].

* Corresponding author.

E-mail addresses: jiratj@tiger.vscht.cz (J. Jirát), kubicek@vscht.cz (M. Kubíček), marek@vscht.cz (M. Marek)

0920-5861/99/$ – see front matter
PII: S0920-5861(99)00146-7

'Oxygen storage' properties of Ce oxides are well known and are utilized in three-way catalysts [3]. Although mathematical modelling of TWC has been widely used for a long time [4], owing to complexity of the phenomena occuring in the washcoat (e.g. [5]) the quantitative description of deposition has mostly not been included in mathematical description. Under fast changing redox conditions following the control of the air/fuel ratio according to signal of the lambda sensor, accumulation and depletion of oxygen on the catalyst occurs. The Ce oxides serve for O_2 deposition under oxidizing conditions and enable higher conversion of CO and HCs under reducing atmosphere. Siemund et al. [6] proposed a simple way of description of surface deposition. Koltsakis et al. [7] then used the simplified model, considering irreversible chemisorption of oxygen followed by catalyst reduction by CO. They also estimated values of rate parameters from experimental data.

Similarly to oxygen storage properties of Ce oxides the 'NO_x storage' properties of earth-alkaline metal oxides, particularly Ba, are being studied. Ba oxides store NO_x in the oxidizing atmosphere and then allow reduction when reducing conditions occur. The NO_x storage properties of Pt/Al_2O_3 type catalysts were first studied in detail by Takahashi et al. [2] and by Bögner et al. [8] and are subject of a number of patents, cf. e.g. [9].

Even if experimental studies of BaO containing catalysts are numerous [10–13] no modelling study of dynamic behavior of NO_x storage catalysts has been described in the open literature. Considering relatively complex proposed mechanism of NO_x storage and reduction [13], it would be more precise to consider full non-stationary kinetics similar to what has been described by Forzatti et al. [14] for catalytic reduction of NO_x by ammonia or by Tagliaferri et al. [15] or Nievergeld et al. [16] for automobile exhaust gas. However, dynamic experimental data for NO_x storage and reduction on Pt/Al_2O_3 are not available, therefore, we cannot evaluate necessary kinetic parameters and use full non-stationary model. Hence, we shall use semiempirical kinetic relations based on quasistationary state assumptions similarly as it has been used for the description of oxygen storage, cf. [7].

A versatile software package for dynamic simulation of interconnected systems of reactors and adsorbers was developed in our laboratory [17],[18]. Model of each unit is described by an appropriate system of PDEs. A mutual heat exchange among individual units and time variable course of inlet variables and parameters can be considered. The software enables to compute simply time periodic operations (e.g. reversal of flow direction) and it can be used both for simulations and also as a subroutine in the software for adaptive control or optimal design. It can also serve as a subroutine for parameter estimation in dynamic experiments. The above software was used for modelling of electrically heated monoliths in the cold-start problem [19], description of the sequence of monoliths with adaptive flow-direction reversal [20], the reactor and adsorber system (HC-trap) [18], periodic operation of thermally coupled monoliths for NO_x reduction under lean conditions [21] and an adaptive control based on neural net prediction of the system of monoliths with time-variable inlet conditions [22]. Here we shall use this software for a dynamic simulation of monolith (and the systems of monoliths) with considered O_2 and NO_x deposition on the washcoat. We shall demonstrate that periodic switching between lean and rich phase on the monolith with proper storage parameters can enable to reach high conversion of NO even under average lean conditions.

2. Problem formulation

2.1. Model equations for a single monolith

A 1-D two-phase pseudo-continuous model [20] has been used for the simulation of typical monolithic reactor. It is represented by the following equations:

2.1.1. Enthalpy balance — gas phase

$$\rho c_p \frac{\partial T}{\partial \tau} = -v\rho c_p \frac{\partial T}{\partial z} - k_{\mathrm{H}}(z)\frac{a}{\varepsilon}(T - T^*) \qquad (1)$$

Here is ρ gas phase density, c_p gas phase heat capacity, T gas phase temperature, τ time, v linear velocity, z axial coordinate, k_{H} heat transfer coefficient, a specific surface area, ε void fraction and T^* solid phase temperature.

2.1.2. Ethalpy balance — solid phase

$$\rho^* c_p^* \frac{\partial T}{\partial \tau} = \lambda_z^* \frac{\partial^2 T^*}{\partial z^2} - \sum_{j=1}^{J} \Delta H_{\mathcal{R}j} \mathcal{R}_j(\vec{c}^*, T^*) - k_H(z) \frac{a}{1-\varepsilon}(T^* - T) \quad (2)$$

Here is ρ^* density of solid phase, c_p^* heat capacity of solid phase, λ_z^* effective axial heat conductivity, $\Delta H_{\mathcal{R}j}$ reaction enthalpy of the jth reaction, J=9

2.1.3. Mass balance — gas phase

For each component (k=CO, O_2, H_2, C_3H_6, C_3H_8, NO) we use mass balance in the form

$$\frac{\partial c_k}{\partial \tau} = -\frac{\partial (v c_k)}{\partial z} - k_C(z) \frac{a}{\varepsilon}(c_k - c_k^*) \quad (3)$$

Here is c_k gas phase concentration of the kth component, k_C meass transfer coefficient, and c_k^* solid phase concentration of the kth component.

2.1.4. Mass balance — solid phase

For each component (k = CO, O_2, H_2, C_3H_6, C_3H_8, NO) it holds

$$\varepsilon^* \frac{\partial c_k^*}{\partial \tau} = k_C(z) \frac{a}{1-\varepsilon}(c_k - c_k^*) + \sum_{j=1}^{J} v_{k,j} \mathcal{R}_j(\vec{c}^*, T^*) \quad (4)$$

Here is ε^* porosity and $v_{k,j}$ stoichiometric coefficient of the kth component in the jth reaction.

2.1.5. Surface deposition

The rate of change of relative fractions of the stored oxygen (ψ_{Ox}) and nitrogen oxide (ψ_{NO}) at the surface considers the rate of storage (adsorption) and reduction related to the corresponding storage capacity of individual components

$$\frac{\partial \psi_{Ox}}{\partial \tau} = -\frac{R_{Ox,red}}{\psi_{Ox,cap}} + \frac{R_{Ox,ads}}{\psi_{Ox,cap}} \quad (5)$$

$$\frac{\partial \psi_{NO}}{\partial \tau} = -\frac{R_{NO,red}}{\psi_{NO,cap}} + \frac{R_{NO,ads}}{\psi_{NO,cap}} \quad (6)$$

Here R_{ads} and R_{red} are rates of deposition and reduction, respectively, and ψ_{cap} are storage capacities for individual components.

2.1.6. Boundary conditions

$$z = 0: \quad T(0,\tau) = T_0, \quad \frac{\partial T^*}{\partial z}(0,\tau) = 0,$$
$$c_k(0,\tau) = c_{k0}, \quad k = 1 \ldots K \quad (7)$$

$$z = L: \quad \frac{\partial T^*}{\partial z}(L,\tau) = 0 \quad (8)$$

2.1.7. Initial conditions

$$T(z, \tau = 0) = T_{init}(z) \qquad T^*(z, \tau = 0) = T^*_{init}(z) \quad (9)$$

$$c_k(z, \tau = 0) = c_{k,init}(z)$$
$$c_k^*(z, \tau = 0) = c^*_{k,init}(z) \qquad k = 1 \ldots K \quad (10)$$

$$\psi_{NO}(z, \tau = 0) = \psi_{NO,init}(z)$$
$$\psi_{Ox}(z, \tau = 0) = \psi_{Ox,init}(z) \quad (11)$$

Here $\psi_{Ox,init}$, $\psi_{NO,init}$ denote initial fractions of stored oxygen and nitric oxide, respectively.

This full model includes the description of the rates of deposition of O_2 and NO on the catalyst surface. For a limiting value $\psi_{cap} = 0$ the reaction rates $R_{Ox,ads} = R_{Ox,red} = R_{NO,ads} = R_{NO,red} = 0$, and the model reduces into the model without deposition (Eq. (5)) and Eq. (6) are omitted in this in this case). The heat and mass transfer coefficients k_H, k_C are functions of axial distance, describing empirically the entrance effects [23].

The system of PDEs was simulated by the universal software discussed above.

3. Reaction scheme with O_2 and NO deposition

We have used the following simplified model reaction scheme, considering NO reduction by CO in a gasoline lean burn engine. Here propylene represents easy-to-oxidize HCs and propane difficult-to-oxidize HCs:

$$CO + \tfrac{1}{2}O_2 \xrightarrow{\mathcal{R}_1} CO_2 \quad (12)$$

$$H_2 + \tfrac{1}{2}O_2 \xrightarrow{\mathcal{R}_2} H_2O \quad (13)$$

$$C_3H_6 + \tfrac{9}{2}O_2 \xrightarrow{\mathcal{R}_3} 3H_2O + 3\,CO_2 \quad (14)$$

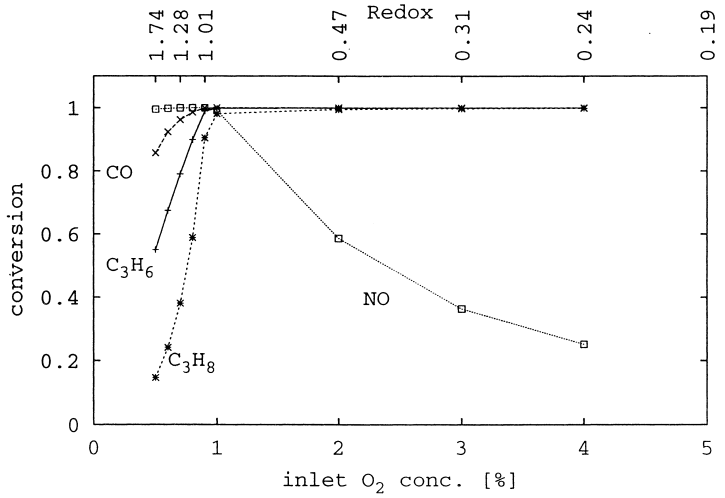

Fig. 1. Steady-state conversions for different inlet O_2 concentration (∼different Redox); only the effects of NO storage were considered.

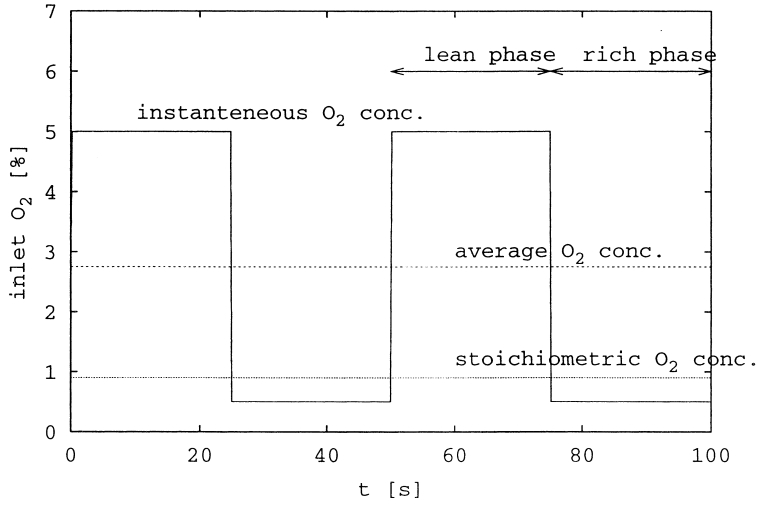

Fig. 2. The course of instantaneous inlet O_2 concentration (switching between 0.5 and 5%.)

$$C_3H_8 + 5O_2 \overset{\mathcal{R}_4}{\rightarrow} 4H_2O + 3CO_2 \quad (15)$$

$$2CO + 2NO \overset{\mathcal{R}_5}{\rightarrow} N_2 + 2\,CO_2 \quad (16)$$

For the description of O_2 and NO deposition in the surface layers of the catalyst the following schematic reactions were considered:

$$\tfrac{1}{2}O_2 + L_{Ce} \overset{\mathcal{R}_{Ox,ads}}{\rightarrow} L_{Ce}O \quad (17)$$

$$CO + L_{Ce}O \overset{\mathcal{R}_{Ox,red}}{\rightarrow} CO_2 \quad (18)$$

$$NO + L_{Ba} \overset{\mathcal{R}_{NO,ads}}{\rightarrow} L_{Ba}NO \quad (19)$$

$$CO + L_{Ba}NO \overset{\mathcal{R}_{NO,red}}{\rightarrow} CO_2 + \tfrac{1}{2}N_2 \quad (20)$$

The symbols L_{Ce} and L_{Ba} represent the sites for O_2 and NO deposition, respectively. CO has been chosen as a typical reductant (its content is highest from the available reductants — CO, H_2, C_3H_6, C_3H_8 — in the considered gas composition), although the reduction by H_2 can be faster. We consider reaction heat for Eq. (17) and Eq. (19) to be negligible.

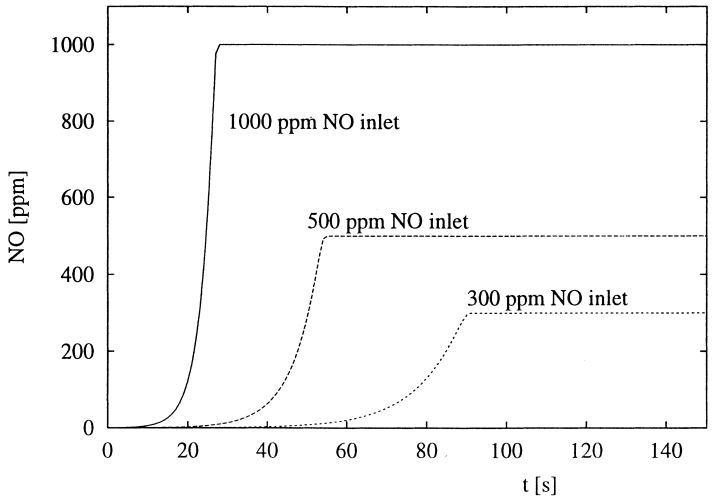

Fig. 3. The outlet NO concentration, only NO deposition considered (no reactions), constant inlet conditions. Initial conditions: $\psi_{NO}(\tau = 0) = 0$.

3.1. Reaction kinetics

The Langmuir–Hinshelwood type reaction expressions Eqs. (21)–(25) proposed already by Voltz et al. [24] are used for the reactions Eqs. (12)–(16), in the form adapted from Koltsakis et al. [7]: (here y denotes surface mole fraction)

$$\mathcal{R}_1 = \frac{k_1 y_{CO} y_{O_2}}{T^* G_1} \quad (21)$$

$$\mathcal{R}_2 = \frac{k_2 y_{H_2} y_{O_2}}{T^* G_1} \quad (22)$$

$$\mathcal{R}_3 = \frac{k_3 y_{C_3H_6} y_{O_2}}{T^* G_1} \quad (23)$$

$$\mathcal{R}_4 = \frac{k_4 y_{C_3H_8} y_{O_2}}{T^* G_1} \quad (24)$$

$$\mathcal{R}_5 = k_5 y_{CO} y_{NO}^{0.5} \quad (25)$$

where $G_1 = (1 + K_1 y_{CO} + K_2 y_{C_3H_6})^2 (1 + K_3 y_{CO}^2 y_{C_3H_6}^2)(1 + K_4 y_{NO}^{0.7})$, $K_1 = 65.5 \exp(961/T^*)$, $K_2 = 2.08 \times 10^3 \exp(361/T^*)$, $K_3 = 3.98 \exp(11611/T^*)$, $K_4 = 4.79 \times 10^5 \exp(-3733/T^*)$. The above semiempirical kinetic relations were derived using the pseudo steady-state approximation, which is in principle not correct for fast transients in inlet conditions. In rigorous description nonstationary kinetic models should be used. However, necessary set of parameters is not available in the required temperature range. For surface deposition the following kinetic relations were used:

$$R_6 = R_{Ox,ads} = k_{Ox,ads}\, y_{O_2}^*\, \psi_{Ox,cap}(1 - \psi_{Ox}) \quad (26)$$

$$R_7 = R_{NO,ads} = k_{NO,ads}\, y_{NO}^*\, \psi_{NO,cap}(1 - \psi_{NO}) \quad (27)$$

$$R_8 = R_{Ox,red} = k_{Ox,red}\, y_{CO}^*\, \psi_{Ox,cap} \psi_{Ox} \quad (28)$$

$$R_9 = R_{NO,red} = k_{NO,red}\, y_{CO}^*\, \psi_{NO,cap} \psi_{NO} \quad (29)$$

where y are molar fractions and the considered reaction rate constants k are of the Arrhenius type. If not stated otherwise the storage capacities considered are $\psi_{Ox,cap} = 10\,mol/m^3$ cat and $\psi_{NO,cap} = 15\,mol/m^3$ cat (this value was estimated from experiments described in [8]). The first order kinetic relation is used for the description of NO deposition (the dependence on oxygen concentration [2] is not explicitly considered). The influence of surface diffusion for the description of such phenomena as a spill-over from Pt sites to Ba sites which have been observed [13], was also not considered. The values of kinetic parameters are in Table 1.

4. Steady-state operation

Let us consider first a standard steady state operation with the following parameters: space velocity

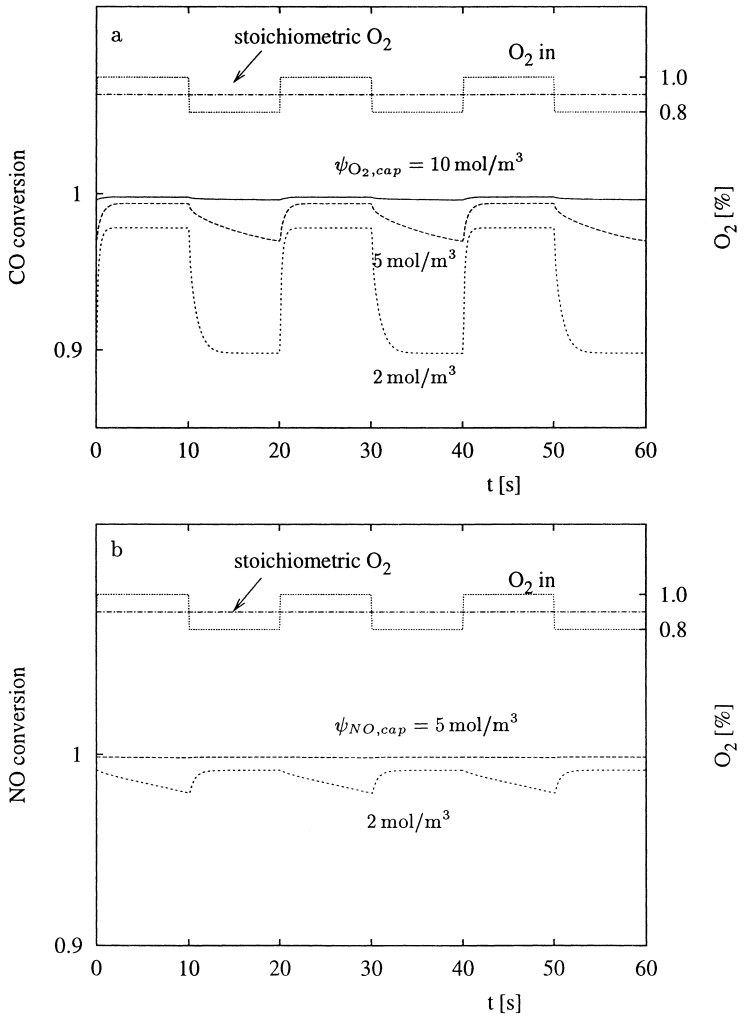

Fig. 4. Effect of O_2 storage capacity on CO conversion and of NO storage capacity on NO conversion. Small oxygen variations around stoichiometric ratio ($y_{O_2,in,rich} = 0.9\%$, Redox = 1). Periodic operation $T_{lean} = T_{rich} = 10$ s.

Table 1
Values of kinetic parameters

Equation	A	E	From references
Eq. (21)	5×10^{16}	95 000	[7]
Eq. (22)	5×10^{16}	95 000	[7]
Eq. (23)	1×10^{18}	105 000	[7]
Eq. (24)	1.2×10^{18}	125 000	[7]
Eq. (25)	1.5×10^{6}	70 000	[7]
Eq. (26)	9×10^{8}	90 000	[7]
Eq. (27)	9×10^{10}	90 000	
Eq. (28)	3×10^{8}	90 000	[7]
Eq. (29)	3×10^{7}	90 000	

Table 2
Inlet gas composition

Component	Inlet concentration
CO	1.1%
H_2	0.37%
C_3H_6	320 ppm
C_3H_8	160 ppm
NO	0.1%
O_2	0.5–5%

60 000/h, reactor (monolith) length 0.11 m, temperature of the inlet gas 400°C and the inlet gas

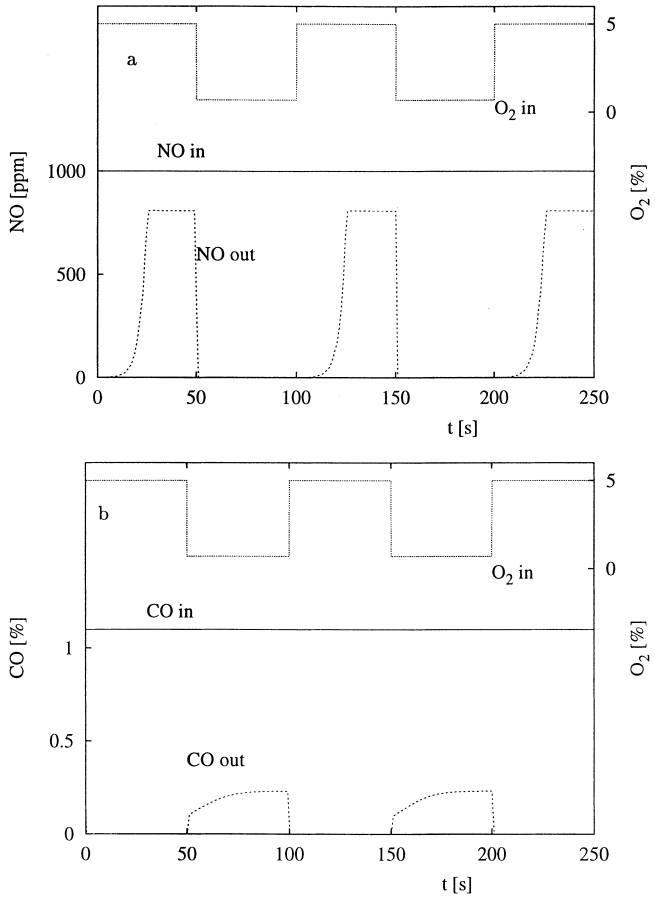

Fig. 5. Stationary time course of the outlet NO (a) and CO (b) concentration. Periodic operation $T_{lean} = T_{rich} = 50\,s$.

composition given in Table 2. The selectivity towards NO reduction is strongly influenced by oxygen content. In typical gasoline engines, the ratio of reducing and oxidizing components (the so-called redox) is kept equal to 1. In this case, the redox can be defined

$$\text{Redox} = \frac{y_{CO} + y_{H_2} + 9y_{C_3H_6} + 10y_{C_3H_8}}{2y_{O_2} + y_{NO}} \qquad (30)$$

Results of computations for steady-state conditions are shown in Fig. 1. When an excess of reduction components is used (Redox $>$ 1) the NO conversion is complete, but CO and HC are not converted because of the lack of oxygen. At a stoichiometric ratio of reducing and oxidizing components (Redox $= 1$) is the conversion of all components complete, cf. Fig. 1.

5. Periodic operation — lean/rich switching

Let us now consider dynamic operation with a periodic switching between rich and lean conditions. In the lean phase the air/fuel ratio is much higher than the stoichiometric one, the engine works efficiently under an excess of oxygen and NO_x is stored within the surface layers (washcoat) of the catalyst. In the rich phase is the air/fuel ratio less than the stoichiometric one. Deposited NO_x is reduced by CO or HC and removed from the surface (e.g., BaO is regenerated). This phase should be as short as possible as the efficiency of the engine decreases.

The concentration of O_2 during the lean phase was 5%, the concentration during the rich phase was considered as an operation parameter (the stoichiometric

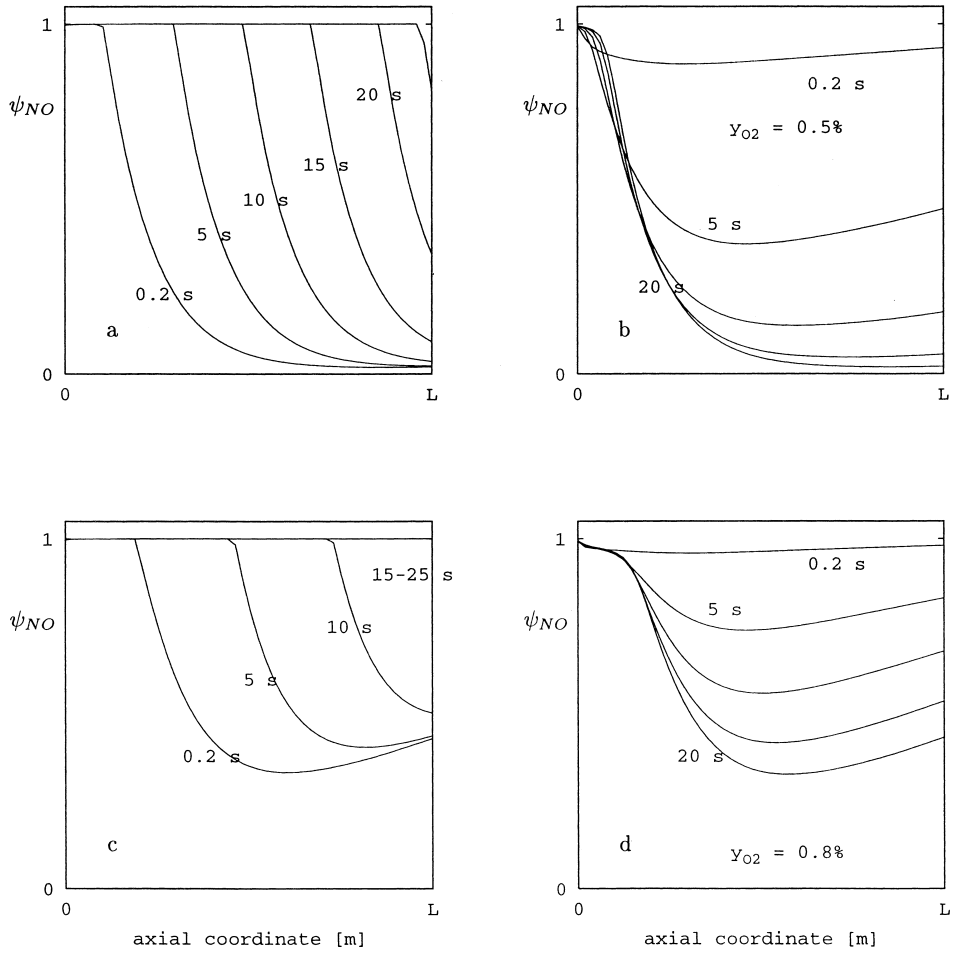

Fig. 6. Profiles of deposited NO. ($T_{\text{lean}} = 25\,\text{s}, T_{\text{rich}} = 20\,s$). Different concentrations of O_2 during the rich phase: 0.5% (a: lean phase, b: rich phase) and 0.8% (c: lean phase, d: rich phase). Time is shown in each figure separately.

O_2 concentration is 0.9%). An example of the time course of the inlet O_2 concentration is depicted in Fig. 2. Our task then is to find the proper operating conditions, e.g., lengths of lean and rich phases which would enable to remove most of CO, HC and NO_x emissions together with the maximum acceptable ratio of lean/rich phases. Let us define average conversion per period (for comparison between periodic and steady state operation) of the kth component in the non-stationary regime as follows:

$$1\text{-}\left(\int_{\tau}^{\tau+T_{\text{lean}}+T_{\text{rich}}} F_{k,\text{out}}\,\mathrm{d}\tau \Big/ \int_{\tau}^{\tau+T_{\text{lean}}+T_{\text{rich}}} F_{k,\text{in}}\,\mathrm{d}\tau\right)$$

where T_{lean} respectively, T_{rich} is the part of whole period with an excess respectively a lack of oxidizing components and F_k denotes molar flux of the kth component.

The periodic operation will be effective only if the length of the lean period (NO storage) will not be too long. The maximum allowable length of the lean phase for given storage capacity and NO_{in} concentration can be estimated from the breakthrough curves, cf. Fig. 3. Here, for example, for NO_{in} equal to 1000 ppm and the given storage capacity is the estimated maximum length of the lean period approximately equal to 25 s.

When the air/fuel ratio is controlled by the signal of the lambda sensor, small fluctuations of O_2

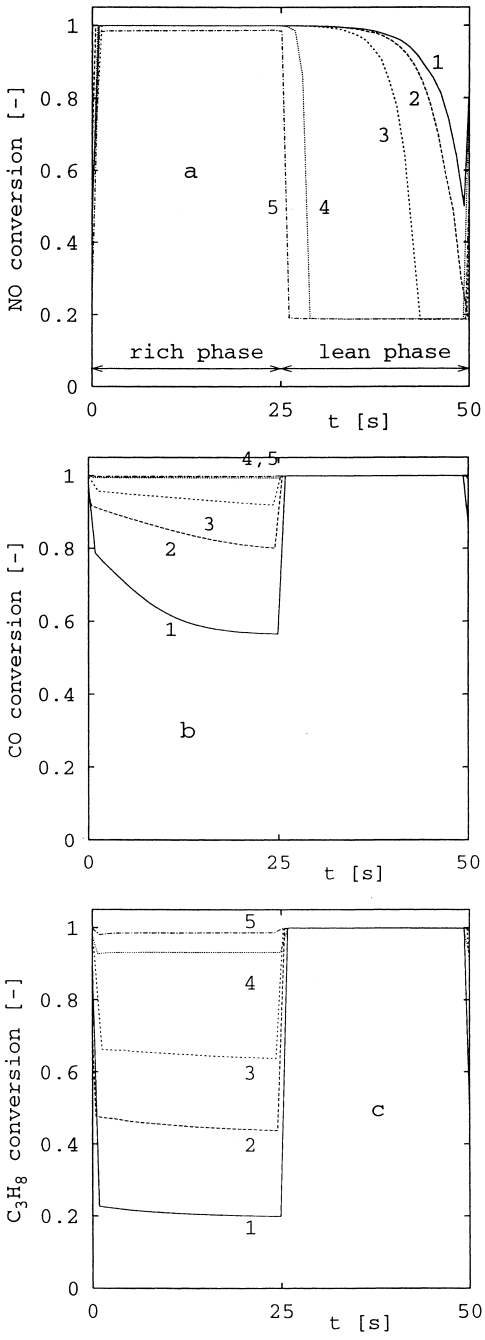

Fig. 7. Dependence of an instantaneous conversion on time. The lean and rich phase length are equal ($T_{lean} = T_{rich} = 25$ s). Different concentrations of O_2 during the rich phase: 1–0.5%, 2–0.7%, 3–0.8%, 4–0.9%, 5–1.0%. During the lean phase is the real conversion of NO very low, the apparent conversion is caused by NO adsorption.

concentration around stoichiometric ratio occur. The effects of storage properties for small variations of O_2 concentration around stoichiometric ratio on conversion are shown in Fig. 4. Hence a proper capacity for O_2 and NO_x storage may improve conversion of both CO and NO also under standard nearly stationary operation and as it follows from detailed simulations, the NO storage capacity $\psi_{NO,cap} \geq 5$ leads to total conversion of NO in this case.

The desired mode of operation is switching between a large period of lean operation with a very high oxygen excess and a small rich period with a mildly reducing conditions. Typical time course of CO and NO outlet concentrations is shown in Fig. 5. During the lean phase, $\tau \in \langle 0; 50 \rangle$, is certain amount of NO stored (cf. Fig. 5a), but the available capacity is low and thus breakthrough of NO occurs. The conversion of CO is at the same time complete (cf. Fig. 5b). Under rich conditions, $\tau \in \langle 50; 100 \rangle$, is the NO storage capacity regenerated and practically no NO emissions occur (cf. Fig. 5a). However, due to the lack of oxygen the conversion of CO is not complete (cf. Fig. 5b).

A parametric study aimed at the minimization of CO and NO_x emissions was performed. The following parameters were varied in simulations: the length of both phases, T_{lean}, T_{rich} (15–150 s) and the inlet O_2 concentration during the rich phase 0.5–1% (Redox= 1.7–0.9).

The evolution of profiles of deposited NO in periodic steady-state for two different rich phase oxygen levels is shown in Fig. 6. Higher O_2 concentration during the rich (regeneration) phase reduces available NO storage capacity in the following lean phase. The storage centra are thus not fully regenerated and the NO breakthrough in the lean phase occurs much earlier.

Typical time course of instantaneous conversions in stationary state is shown in Fig. 7 for several values of O_2 inlet concentration in the rich phase. The actual values of conversion of CO and HCs in the rich phase and hence also the time-averaged conversions decrease with the decreasing $(O_2)_{in}$. On the other hand the conversions of NO in the lean phase increase (caused by NO deposition on the surface). Results of periodic switching operation can be compared with those obtained for standard stationary operation: e.g., for an average O_2 concentration ($y_{O_2,in,avg}$) 2.9% is the steady-state conversion $\bar{x}_{NO}$ approx. 40% (see

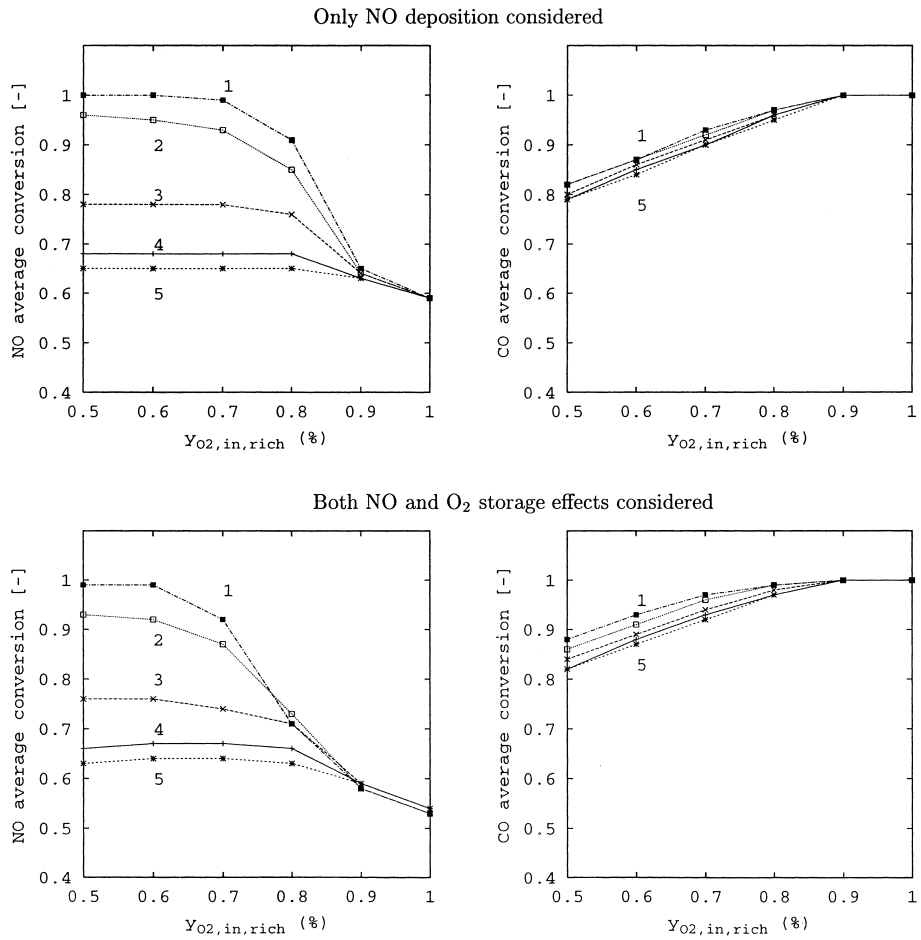

Fig. 8. Average CO and NO conversions (averaged over both rich and lean phases) vs. $y_{O_2,in,rich}$ (the inlet O_2 concentration during the rich phase). In this case are the lean and rich phase lengths equal $T_{lean} = T_{rich}$: 15 (1), 25 (2), 50 (3), 100 (4), 150 s (5).

Fig. 1), while for the periodic one is the best obtained NO_x conversion $\bar{x}_{NO}$ higher than 90% (see Fig. 7, to $y_{O_2,in,avg}$ =2.9% corresponds $y_{O_2 in,rich}$ =0.8%).

The dependences of average conversions on the inlet O_2 concentration are depicted in Fig. 8 for different periods. The higher is the O_2 concentration in the course of the rich phase, the lower are time averaged NO conversions and the higher the time averaged CO conversions. The O_2 deposition improves the conversion of CO but decreases NO reduction.

Let us consider a periodic switching operation with an unequal length of lean and rich periods, $T_{lean} \neq T_{rich}$. For given values of the inlet NO concentration and the considered NO storage capacity we can find from Fig. 3 that the length of the lean phase should not exceed ~25 s. Thus the length of the lean phase (T_{lean}) was taken constant, equal to 25 s, and the length of the rich phase (T_{rich}) and the inlet O_2 concentration during the rich phase were varied. The resulting time averaged conversions are shown in Fig. 9. The trends are obvious — the shorter the rich (regeneration) period the higher is $\bar{x}_{CO}$ and the lower is $\bar{x}_{NO}$. The O_2 deposition again improves conversion of CO and decreases NO reduction.

The above-described periodic operation can cause lower values of actual CO and HC conversions to occur in the course of even very short rich phase. To increase NO conversion without an increase of CO and

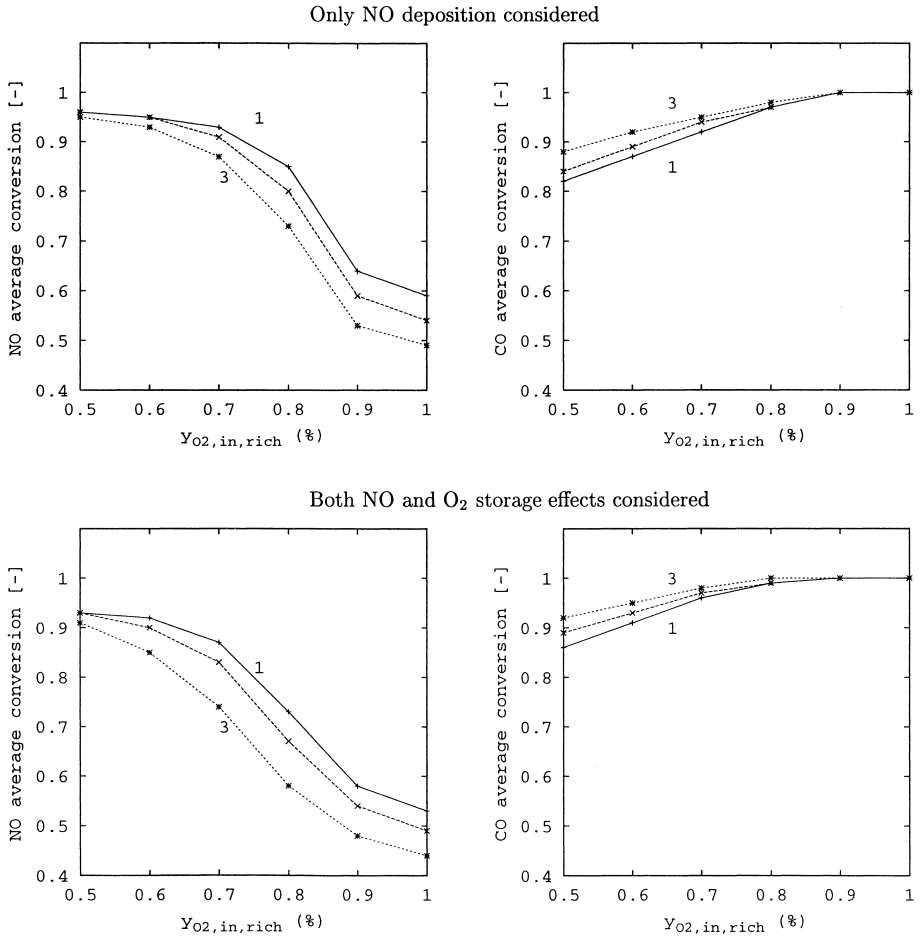

Fig. 9. Average CO and NO conversions (averaged over both rich and lean phases) vs. $y_{O_2,in,rich}$ (the inlet O_2 concentration during the rich phase). $T_{lean} = 25$ s, $T_{rich} = 25$ (1), 20 (2), 15 s (3).

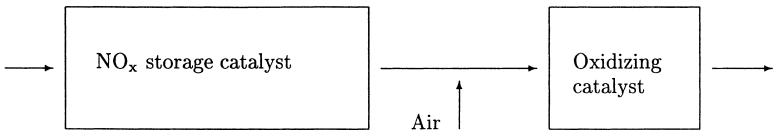

Fig. 10. System of two reactors — the first monolith stores NO_x under lean conditions (NO_x is removed under rich conditions). The second (oxidizing) monolith burns CO and HC during the rich phase.

HC emissions during the rich phase two monoliths can be used (cf. Fig. 10). The first monolith has NO_x storage properties (for NO_x removal), the second one is only oxidizing. Additional air is injected in front of the oxidizing catalyst to ensure a sufficient excess of oxygen. Similar system was described already many years ago [25]. Examples of conversion and concentration profiles during both lean and rich phases in such arrangement are shown in Figs. 11 and 12. The outlet CO conversion is complete (due to injected air the conditions in the second reactor are always lean). NO_x conversion depends on the used settings of operating parameters (T_{rich}, T_{lean}, $y_{O_2,in,rich}$) and is not affected by the presence of the second monolith.

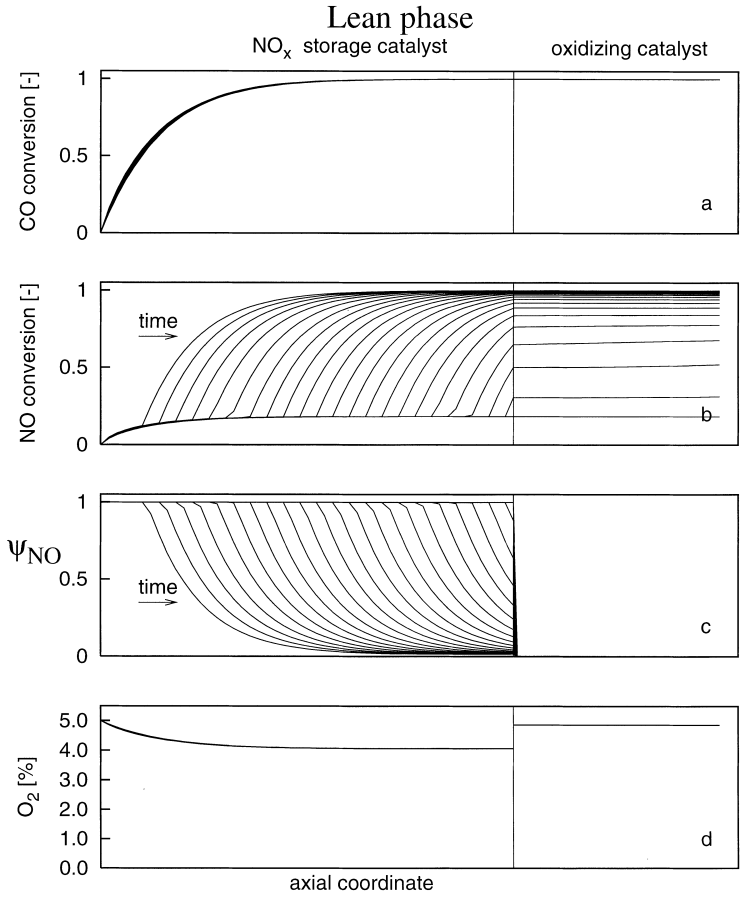

Fig. 11. Conversion and concentration profiles during the lean phase, T_{lean} =25 s, T_{rich} = 20 s, $y_{O_2,in,rich}$ =0.05%. CO is completely oxidized already in the first catalyst. NO conversion is only apparent and is caused by NO deposition on the surface (cf. b and c). Oxygen level is high in both reactors.

6. Conclusions

Parametric study of a catalytic monolithic reactor treating exhaust gases from a gasoline lean-burn engine operating periodically under rich and lean conditions with O_2 and NO_x surface deposition has shown that it is possible for proper operating and catalyst parameters to achieve nearly complete CO and NO conversions, even in the case where the time-average O_2 concentration is three times higher than the stoichiometric one. The model used enables also to estimate the suboptimal operating parameters for different adsorbent capacities and inlet conditions. The developed software can also be used for fitting of kinetic parameters to experimental data. For example, the breakthrough experiments (cf. Fig. 3) can be used for evaluation of storage parameters and the time course of outlet concentrations of periodically operated monoliths can serve for an evaluation of deposition and reduction dynamics.

7. Notation

a	specific surface, m^{-1}
c	fluid phase concentration, mol m^{-3}
c^*	solid phase concentration, mol m^{-3}
c_p	fluid phase heat capacity, J kg^{-1} K^{-1}
c_p^*	solid phase heat capacity, J kg^{-1} K^{-1}

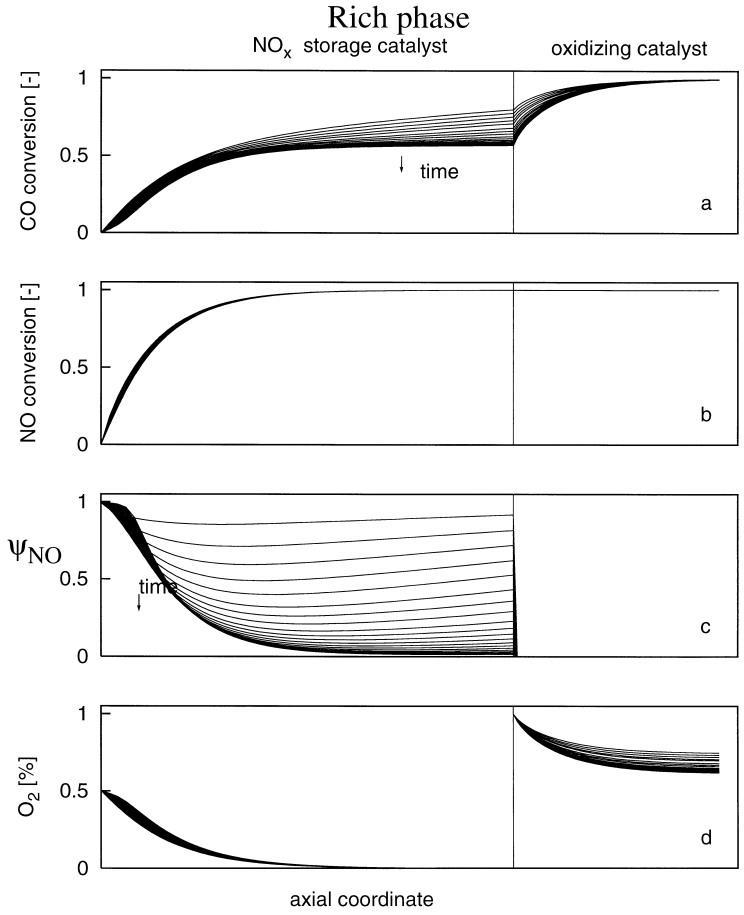

Fig. 12. Conversion and concentration profiles during the rich phase, T_{lean} =25 s, T_{rich} =20 s, $y_{O_2,\text{in,rich}}$ =0.05%. CO is completely oxidized in the second monolith by an injected additional air (cf. a and d). NO conversion is complete in the first monolith (cf. b) and the NO_x storage material is regenerated (cf. c). Conditions in the first monolith are reducing, in the second one oxidizing.

k_C	mass transfer coefficient, m s^{-1}
k_H	heat transfer coefficient, J m^{-2} s^{-1} K^{-1}
$k_1 \ldots k_4$	reaction rate constants, mol m^{-3} s^{-1} K
k_5	reaction rate constant, mol m^{-3} s^{-1}
k_{ads}, k_{red}	deposition and reduction rate constants, s^{-1}
L	reactor length, m
$\mathcal{R}$	reaction rate, mol m^{-3} s^{-1}
T	fluid temperature, K
T^*	solid phase temperature, K
v	gas velocity, m s^{-1}
x	conversion
y	mole fraction
z	axial coordinate, m
ΔH_R	reaction enthalpy, J mol^{-1}
ρ	fluid density, kg m^{-3}
ρ^*	solid phase density, kg m^{-3}
ε	void fraction
ε^*	porosity
λ_z^*	solid phase axial heat conductivity, J m^{-1} s^{-1} K^{-1}
v_{kj}	stoichiometric coefficient of the kth component in the jth reaction, (for reactants < 0)
ψ_{cap}	storage capacity, mol m^{-3} solid
ψ	fraction of occupied storage sites
τ	time, s

Acknowledgements

The authors are thankful to anonymous referees for suggestions which improved the presentation in the paper. This work was partially supported by the Grant No. 104/97/0602, Czech Grant Agency, Grant No. VS96073, Czech Ministry of Education and EU grant CIPA-CT92-4021.

References

[1] A. Fritz, V. Pitchon, Appl. Catal. B 13 (1997) 1.
[2] N. Takahashi, H. Shinjoh, T. Iijima, T. Suzuki, K. Yamazaki, K. Yokota, H. Suzuki, N. Miyoshi, Shin-ichi Matsumoto, T. Tanizawa, T. Tanaka, S. Tateishi, K. Kasahara, Catal. Today 27 (1996) 63.
[3] R.K. Herz, Ind. Eng. Chem. Proc. Res. Dev. 20 (1981) 451.
[4] S.H. Oh, J.C. Cavendish, AIChE J. 26 (1985) 935.
[5] T. Bunluesin, R.J. Gorte, G.W. Graham, Appl. Catal. B 14 (1997) 105.
[6] S. Siemund, D. Schweich, J.P. Leclerc, J. Villermaux, Stud. Surf. Sci. Catal. 96 (1995) 887.
[7] G.C. Koltsakis, P.A. Konstantinidis, A.M. Stamatelos, Appl. Catal. B 12 (1997) 161.
[8] W. Bögner, M. Krämer, B. Krutzsch, S. Pischinger, D. Voigtländer, G. Wenninger, F. Wirbeleit, M.S. Brogan, R.J. Brisley, D.E. Webster, Appl. Catal. B 7 (1995) 153.
[9] K. Yamasita, M. Sugiyama, M. Murachi, EP 754494 A2.
[10] E. Fridell, M. Skoglundh, S. Johansson, B. Westerberg, A. Törncrona, G. Smedler, Stud. Surf. Sci. Catal. 116 (1998) 537.
[11] N. Fekete, R. Kemmler, D. Voigtländer, B. Krutzsch, E. Zimmer, G. Wenninger, W. Strehlau, J.A.A. Van Den Tillaart, J. Leyrer, Soc. Automot. Eng. SP-1248, p. 249.
[12] H. Shinjoh, N. Takahashi, K. Yokota, M. Sugiura, Appl. Catal. B 15 (1998) 189.
[13] N. Takahashi, K. Yokota, M. Sugiura, in: Proc. 2nd World Congress on Environmental Catalysis 1998, Miami Beach, FL, USA, 15–20 November 1998.
[14] P. Forzatti, L. Lietti, C. Orsenigo, L. Nova, E. Tronconi, in: Proc. 2nd World Congress on Environmental Catalysis 1998, Miami Beach, FL, USA, 15–20 November 1998.
[15] S. Tagliaferri, L. Padeste, A. Baiker, Stud. Surf. Sci. Catal. 96 (1995) 897.
[16] A.J.L. Nievergeld, J.H.B.J. Hoebink, G.B. Marin, Stud. Surf. Sci. Catal. 96 (1995) 909.
[17] M. Kubíček, P. Pinkas, J. Jirát, D. Šnita, M. Marek, Comput. Chem. Eng. 21 (1997) S757.
[18] F. Štěpánek, J. Jirát, M. Kubíček, M. Marek, in: Proc. 2nd World Congress on Environmental Catalysis 1998, Miami Beach, FL, USA, 15–20 November 1998, p. 537.
[19] P. Pinkas, D. Šnita, M. Kubíček, M. Marek, Chem. Eng. Sci. 49 (1994) 5347.
[20] P. Pinkas, D. Šnita, M. Kubíček, M. Marek, Chem. Eng. Sci. 51 (1996) 3157.
[21] J. Jiràt, F. Štěpànek, M. Kubìček, M. Marek, Chem. Eng. Sci. 54 (1999) 2609.
[22] F. Štěpànek, J. Jiràt, M. Kubìček, M. Marek, Compnt. Chem Eng. 23 (1999) S317.
[23] T. Kirchner, D. Eigenberger, Chem. Eng. Sci. 51 (1996) 2409.
[24] S.E. Voltz, C.R. Morgan, D. Liederman, S.M. Jaco, Ind. Eng. Chem. Proc. Res. Dev. 12 (1973) 295.
[25] J.C. Summers, D.R. Monroe, Ind. Eng. Chem. Proc. Res. Dev. 20 (1981) 23.